

Article

Effects of the Carbon Support Doping with Nitrogen for the Hydrogen Production from Formic Acid over Ni Catalysts

Alina D. Nishchakova ¹, Dmitri A. Bulushev ^{1,2,3} , Olga A. Stonkus ^{2,3}, Igor P. Asanov ^{1,3} , Arcady V. Ishchenko ^{2,3}, Alexander V. Okotrub ^{1,3} and Lyubov G. Bulusheva ^{1,3,*} 

¹ Laboratory of Physics & Chemistry of Nanomaterials, Nikolaev Institute of Inorganic Chemistry, SB RAS, 630090 Novosibirsk, Russia; nishchakova@niic.nsc.ru (A.D.N.); dmitri.bulushev@catalysis.ru (D.A.B.); asan@niic.nsc.ru (I.P.A.); spectrum@niic.nsc.ru (A.V.O.)

² Borekov Institute of Catalysis, SB RAS, 630090 Novosibirsk, Russia; stonkus@catalysis.ru (O.A.S.); arkady.ishchenko@gmail.com (A.V.I.)

³ Department of Natural Sciences, Novosibirsk State University, 630090 Novosibirsk, Russia

* Correspondence: bul@niic.nsc.ru; Tel.: +7-383-330-5352

Received: 30 September 2019; Accepted: 23 October 2019; Published: 28 October 2019



Abstract: Porous nitrogen-doped and nitrogen-free carbon materials possessing high specific surface areas (400–1000 m² g⁻¹) were used for deposition of Ni by impregnation with nickel acetate followed by reduction. The nitrogen-doped materials synthesized by decomposition of acetonitrile at 973, 1073, and 1173 K did not differ much in the total content of incorporated nitrogen (4–5 at%), but differed in the ratio of the chemical forms of nitrogen. An X-ray photoelectron spectroscopy study showed that the rise in the synthesis temperature led to a strong growth of the content of graphitic nitrogen on the support accompanied by a reduction of the content of pyrrolic nitrogen. The content of pyridinic nitrogen did not change significantly. The prepared nickel catalysts supported on nitrogen-doped carbons showed by a factor of up to two higher conversion of formic acid as compared to that of the nickel catalyst supported on the nitrogen-free carbon. This was related to stabilization of Ni in the state of single Ni²⁺ cations or a few atoms clusters by the pyridinic nitrogen sites. The nitrogen-doped nickel catalysts possessed a high stability in the reaction at least within 5 h and a high selectivity to hydrogen (97%).

Keywords: nickel catalyst; porous carbon support; nitrogen doping; formic acid decomposition; hydrogen production

1. Introduction

Currently, hydrogen is one of the most promising substances that can replace usable sources of energy like natural gas or oil because it is ecologically pure and can be produced from renewable sources. At the same time, hydrogen usage has difficulties associated with its storage and transportation. That is why hydrogen production from different organic compounds with a relatively high content of hydrogen is a current trend in catalysis. Formic acid is a liquid organic hydrogen carrier containing 4.4 wt% of hydrogen, which can be liberated relatively easy using some catalysts. It is important that formic acid can be produced from biomass or CO₂ [1,2].

The most efficient catalysts for the hydrogen production from formic acid are based on palladium. However, noble metals are expensive and this is a reason for searching cheaper catalysts. Such catalysts could be based on Mo sulfide [3,4] or carbide [5], copper [6,7], or nickel [8–10].

Catalysts' supports may play an important role for catalytic activity especially when a highly dispersed active metal is used. Porous carbon materials are suitable candidates, since they have all the

qualities that a support should possess. These materials demonstrate chemical, thermal, and mechanical stability and have a developed surface, which can be modified during the synthesis or post-synthetic processing by doping with heteroatoms like nitrogen [11,12]. They are usually cheap to synthesize and they are easy to handle. Our earlier results demonstrated a significant promotion of Pd catalysts by nitrogen doping of the carbon support for the gas-phase formic acid decomposition reaction [13]. This was related to the formation of new active sites—single Pd cations attached to pyridinic nitrogen species of the support. For the liquid phase decomposition, the nitrogen-doping played also a positive role [14,15].

Nickel is able to form single Ni atoms (cations) on the surface of nitrogen-doped carbon [16], which could be the active sites for some hydrogenation [17] and CO₂ electroreduction [18–21] reactions. It is not known whether these Ni species can be active in the formic acid decomposition reaction. Only theoretical grounds exist that single Ni cations inserted into carbon-nitrogen layer of the C₂N stoichiometry could be active in this reaction [22] providing energy barriers for the reaction steps comparable with those for Pt or Pd catalysts. Hence, the objective of our research was development of porous nitrogen-doped carbon supports for Ni catalysts of the hydrogen production from formic acid. Therefore, the decomposition of formic acid on four catalytic systems consisting of Ni deposited on the surfaces of porous nitrogen-doped and nitrogen-free carbon materials was studied.

2. Materials and Methods

2.1. Materials Synthesis

Porous carbon supports were synthesized using the chemical vapor deposition (CVD) method that is described in detail elsewhere [23]. The horizontal tubular quartz reactor was pumped out, filled with argon, and heated to the required temperature. Calcium tartrate doped with Fe (0.5 at%) was placed in the hot zone of the reactor for 420 s to produce template particles. After that, vapors of acetonitrile, taken as the source of nitrogen-doped carbon materials, or ethanol, used for the nitrogen-free material synthesis, were fed for 0.5 h. The product was kept in an HCl solution for 24 h, washed with distilled water on a polypropylene filter to pH = 7, and dried in an oven for an hour at 373 K. The synthesis was carried out at temperatures 973, 1073, and 1173 K and the obtained samples are referred to CN-973, CN-1073, CN-1173, and C-1073, where “CN” and “C” indicate the presence/absence of nitrogen atoms in the structure and “973”, “1073”, and “1173” is the synthesis temperature.

Heterogeneous nickel catalysts were synthesized by impregnation method: nickel precursor—Ni(OAc)₂ × 4H₂O (8.6 mg) was dissolved in tetrahydrofuran (6 mL) by stirring for 1200 s at room temperature. Then, the support (0.2 g) was added and the mixture was stirred for 4 h at 333 K. After that, tetrahydrofuran was removed by evaporation at room temperature. To decompose nickel acetate, the obtained pre-catalyst was heated at 623 K in an argon flow for 0.5 h and then cooled to room temperature without air access. All the weights were chosen to correspond to 1 wt% of deposited nickel.

2.2. Instrumental Methods

X-ray photoelectron spectroscopy (XPS) experiments were performed on a laboratory PHOIBOS 150 (SPECS GmbH, Berlin, Germany) spectrometer. Monochromatic radiation of the AlK α line (1486.7 eV) was used as an excitation source. An analysis of the porous structure was performed using an Autosorb iQ (Quantachrome Instruments, Boynton Beach, FL, USA) device at 77 K. A specimen was first treated in dynamic vacuum using standard ‘outgas’ option of the equipment at 373 K during 6 h. N₂ adsorption–desorption isotherms were measured within the range of relative pressures of 10^{−6} to 0.99. Then, specific surface areas were calculated using the Brunauer–Emmett–Teller (BET) method. The transmission electron microscopy (TEM) data were obtained using JEM-2010 and JEM-2200FS (JEOL Ltd., Tokyo, Japan) microscopes operated at 200 kV. Images with a high atomic number contrast were acquired using a high angle annular dark field (HAADF) detector in the Scanning-TEM (STEM)

mode. However, this approach did not allow seeing single Ni atoms. The samples for the study were dispersed in ethanol by ultrasound and deposited on a holey carbon film mounted on a copper grid.

2.3. Catalytic Measurements

Formic acid decomposition was performed in a fixed-bed glass reactor, located in the furnace, using a flow set-up described in [24]. Argon was saturated with formic acid vapors passing through a glass container (bubbler) with liquid formic acid. After an additional dilution with argon, the concentration of formic acid vapor reached 2.5 vol% and the total gas flow rate was equal to 4020 mL s⁻¹. A catalyst was put into the reactor over a piece of quartz wool. Before every catalytic reaction experiment, the catalyst was heated in the same formic acid/Ar flow at 623 K for 0.5 h to reduce Ni and stabilize the catalyst.

Products of the decomposition reaction were analyzed by a Chromos GC-1000 gas chromatograph (Chromos Engineering, Moscow, Russia). The conversion of formic acid (X) was determined as the ratio of the sum of the obtained concentrations of CO and H₂ to the initial concentration of formic acid:

$$X = \frac{C_{\text{CO}} + C_{\text{H}_2}}{C_{\text{HCOOH}}} \times 100\%. \quad (1)$$

From the obtained conversion values, the specific reaction rates (W) were calculated, related to the mass of Ni in the catalyst:

$$W = \frac{X \times C_{\text{HCOOH}} \times V_f \times N_A}{22,400 \times m_{\text{Ni}}} \quad [\text{molecule s}^{-1} \text{g}_{\text{Ni}}^{-1}], \quad (2)$$

where C_{HCOOH} —initial formic acid concentration in the Ar flow, V_f —total flow rate (mL s⁻¹), N_A —the Avogadro constant (is equal to 6.022×10^{23} molecule mol⁻¹), m_{Ni} —Ni mass in the catalyst sample (g), and 22,400—volume of one mole of gas at 273 K and 1 atm (mL mol⁻¹).

3. Results and Discussion

3.1. Characterization of the Supports

A quick thermolysis of calcium tartrate accompanying by release of CO₂ and H₂O gases results in the formation of highly dispersed CaO particles [23]. These particles serve as a template for the growth of graphene-like layers catalyzed by iron incorporated into the template. Removal of CaO by washing of the synthesis product in HCl produces pores of different sizes. BET surface area values changed from 966 m² g⁻¹ for the C-1073 sample to 407 m² g⁻¹ for the CN-1173 sample (Table 1). All the nitrogen-doped carbon supports synthesized from acetonitrile had a lower BET surface area as compared to the nitrogen-free material synthesized from ethanol.

Table 1. Some characteristics of the supports and catalysts.

Support	BET Surface Area, m ² g ⁻¹	Content of N, at% (XPS)	Content of O, at% (XPS)	Catalyst	Mean Ni Particle Size, nm
C-1073	966	–	3.0 ± 0.5	Ni/C-1073	3.9 ± 1.2
CN-973	866	5.2 ± 0.5	6.2 ± 0.5	Ni/CN-973	<3 nm (rarely seen)
CN-1073	443	4.4 ± 0.5	3.2 ± 0.5	Ni/CN-1073	<3 nm (rarely seen)
CN-1173	407	4.6 ± 0.5	2.2 ± 0.5	Ni/CN-1173	5.5 ± 1.5

The nitrogen and oxygen contents in the supports were determined from the ratio of the areas under the C 1s, N 1s, and O 1s peaks in survey XPS data taking into account the photoionization cross-sections for the elements at the given photon energy. The obtained values are collected in Table 1. The content of nitrogen in the nitrogen-containing samples remains almost unchanged, corresponding to ca. 5 at%. The oxygen content in the samples decreases with the synthesis temperature from ca. 6.2 at% in CN-973 to ca. 2.2 at% in CN-1173.

The forms of the incorporated nitrogen were revealed from fitting of the N 1s spectra (Figure 1a). Four components were assigned to pyridinic (398.3 eV), pyrrolic (400.0 eV), graphitic (401 eV), and oxidized (402.5 eV) nitrogen [25]. Graphitic nitrogen atoms replaced the three-coordinated carbon atoms of graphene lattice, while other nitrogen species were formed at graphene edges and vacancies. Relative content of the nitrogen forms in the CN-supports is presented in Figure 1b. The rise of the synthesis temperature caused a decrease of the contents of pyrrolic nitrogen and an increase of the content of graphitic nitrogen, which was the most thermodynamically stable nitrogen form. The content of pyridinic nitrogen did not change significantly with the synthesis temperature.

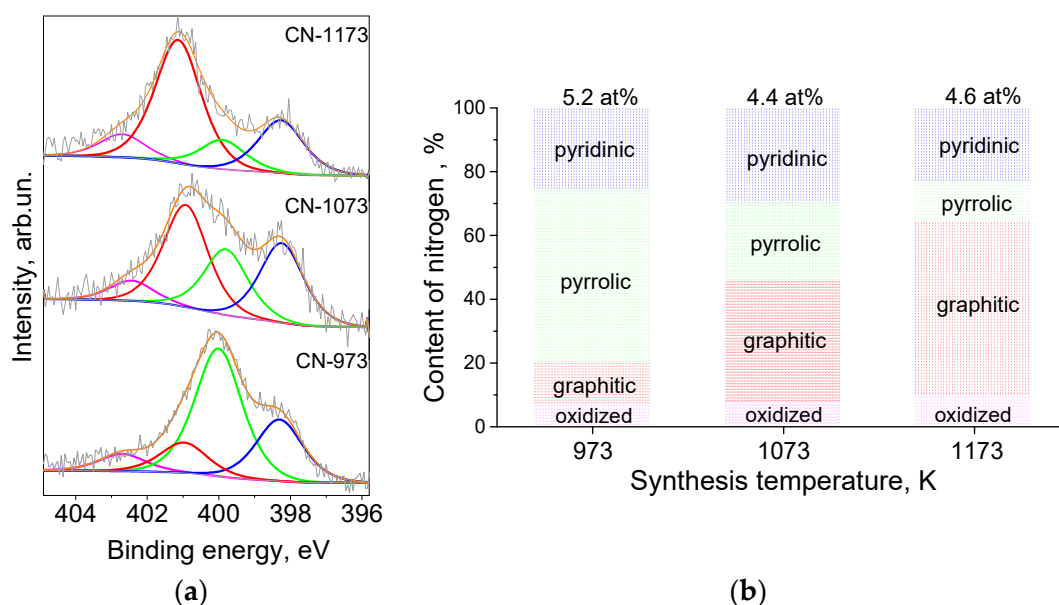


Figure 1. (a) N 1s X-ray photoelectron spectroscopy lines for the catalysts supports and (b) dependences of the content of nitrogen forms on the synthesis temperature.

3.2. Characterization of the Catalysts

Figure 2 shows an HAADF/STEM image of the Ni/C-1073 catalyst after the reaction. The mean particle size in this catalyst determined from these data was 3.9 nm (Table 1). Figure 3 shows TEM images of the Ni catalysts on the nitrogen-doped supports after the reaction. The only catalyst in which Ni containing particles were well seen was Ni/CN-1173. The mean particle size in this catalyst was 5.5 nm. In the Ni/CN-973 and Ni/CN-1073 catalysts, nanoparticles were rare and cannot be clearly seen in TEM images (Figure 3). The HAADF/STEM measurements of the Ni/CN-1073 sample found many extended regions in the sample without nanoparticles like that is shown in Figure 4a. However, the particles with a size smaller than 3 nm could be still found in this sample (Figure 4b,c), but this was a rare case. The smallest nickel species detected by HAADF/STEM had a size of 0.3–0.5 nm (Figure 4c). Hence, it was not possible to plot particle size distributions for these samples. The main part of Ni must be present in a highly dispersed state either in the form of single Ni atoms or few-atom clusters, which were almost not possible to observe by the techniques used. The difference between Ni/CN-1073 and Ni/C-1073 samples could be explained by a strong interaction of single Ni atoms with nitrogen species of the nitrogen-doped supports. In accordance, Zhong et al. [22] using density functional theory (DFT)

calculations showed a strong interaction of a Ni atom with two pyridinic atoms of a C₂N fragment limiting Ni diffusion between different sites of the support and, therefore, preventing Ni sintering.

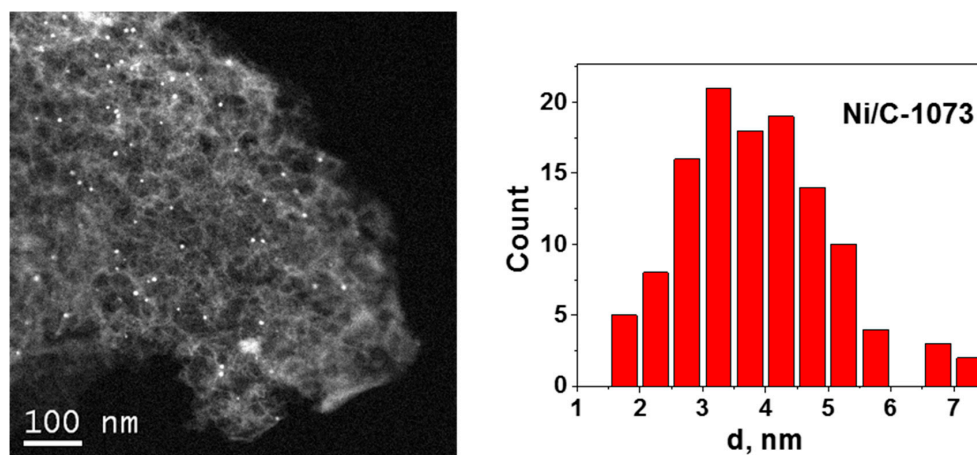


Figure 2. High angle annular dark field/scanning TEM (HAADF/STEM) image of the Ni/C-1073 catalyst after the reaction and Ni particle size distribution for this sample.

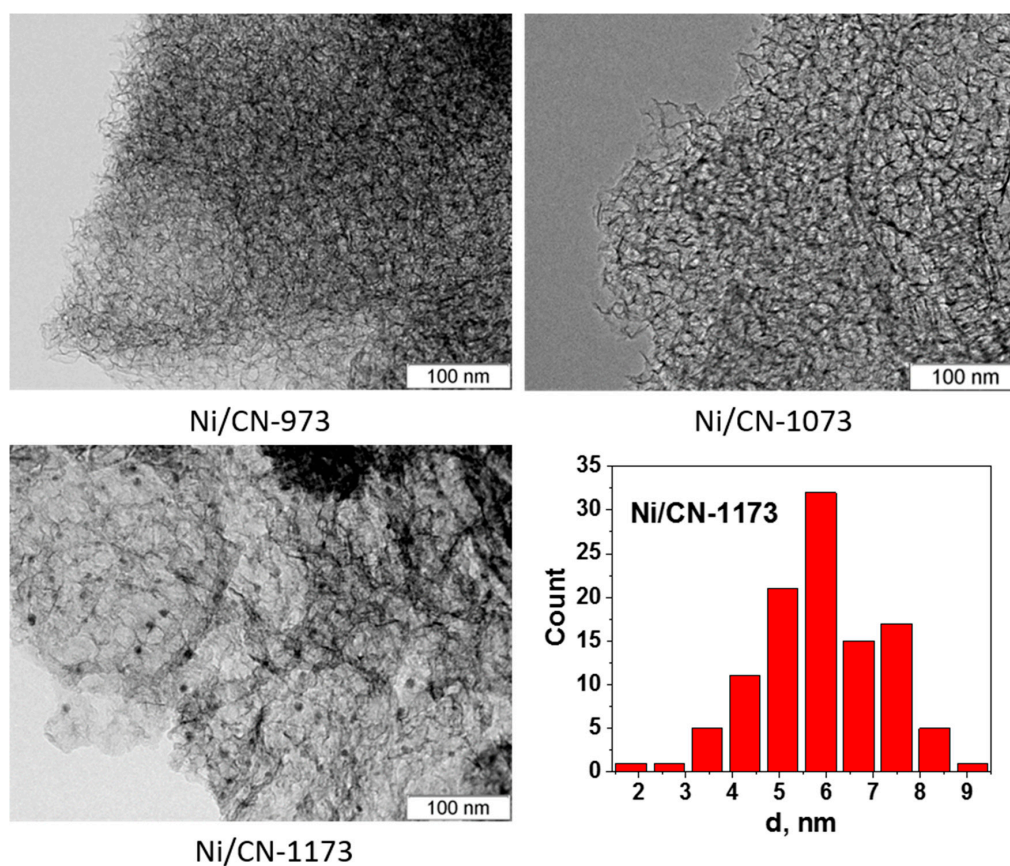


Figure 3. TEM images of the Ni catalysts, which were produced using nitrogen-doped porous carbon materials synthesized at 973 K (Ni/CN-973), 1073 K (Ni/CN-1073) and 1173 K (Ni/CN-1173), after the reaction and Ni particle size distribution for Ni/CN-1173.

Interesting that the increase of the synthesis temperature of the nitrogen-doped carbon up to 1173 K leads to an increase of the mean Ni particle size on the support. It becomes even bigger than that for the Ni/C-1073 catalyst. This could be related to the observed decrease of the content of oxygen and pyrrolic nitrogen species (Table 1). Besides, the TEM data showed that the Ni/CN-1173 sample has a smoother surface than the other two nitrogen-doped samples. The better graphitization of the support in the former case was due to the higher temperature of the material synthesis. This could be also a reason of the bigger size of Ni nanoparticles in the Ni/CN-1173 sample as compared to those in the Ni/CN-973 and Ni/CN-1073 samples. The observed change in the BET surface area should be also taken into account for explanation of the difference in the Ni dispersion for the Ni/C-1073 and Ni/CN-1173 samples.

The Ni $2p_{3/2}$ lines obtained by XPS for all catalysts are compared in Figure 5. It is seen that the binding energies of the Ni $2p_{3/2}$ lines differ for the nitrogen-doped and nitrogen-free catalysts. Thus, the position for the nitrogen-free catalyst corresponds to 856.3 eV while those for the nitrogen-doped catalysts synthesized at 973 and 1073 K are by about 1 eV lower (855.3 eV). Both positions should be assigned to oxidized Ni state (Ni^{2+}). Yamada et al. [16] assigned nickel with the Ni $2p_{3/2}$ binding energy at 855.5 eV to Ni cations interacting with pyridinic nitrogen atoms of the nitrogen-doped carbon support while that at 856.2 eV to $Ni(OH)_2$ and Ni interacting with oxygen containing functional groups, which are also presented in our nitrogen-free carbon support (Table 1). Similarly, Liu et al. [17] assigned their 855.3 eV line to single Ni cations attached to pyridinic nitrogen species of the nitrogen-doped carbon support since the catalyst did not contain nickel in the form of nanoparticles, but contained nickel only in the state of single atoms according to extended X-ray absorption fine structure (EXAFS) and HAADF/STEM data. This binding energy is also typical for different nickel(II) porphyrin derivatives [26]. The line at 855.3–855.5 eV was the most clearly seen for the Ni/CN-1073 sample implying that single Ni^{2+} cations attached to pyridinic nitrogen were the main species representing Ni in this catalyst. The line at 856.3 eV for the nitrogen-free Ni/C-1073 catalyst should be assigned mainly to $Ni(OH)_2$ in the nanoparticles observed by HAADF/STEM (Figure 2). The intermediate binding energy for the Ni/CN-1173 catalyst was explained by the presence of both Ni^{2+} species.

Hence, the electronic state of Ni in the nitrogen-doped catalysts differed from that in the nitrogen-free catalyst indicating interaction of Ni with nitrogen sites of the support. The nitrogen-doped catalysts mainly contained single Ni^{2+} cations attached to pyridinic nitrogen species of the support in agreement with the literature data.

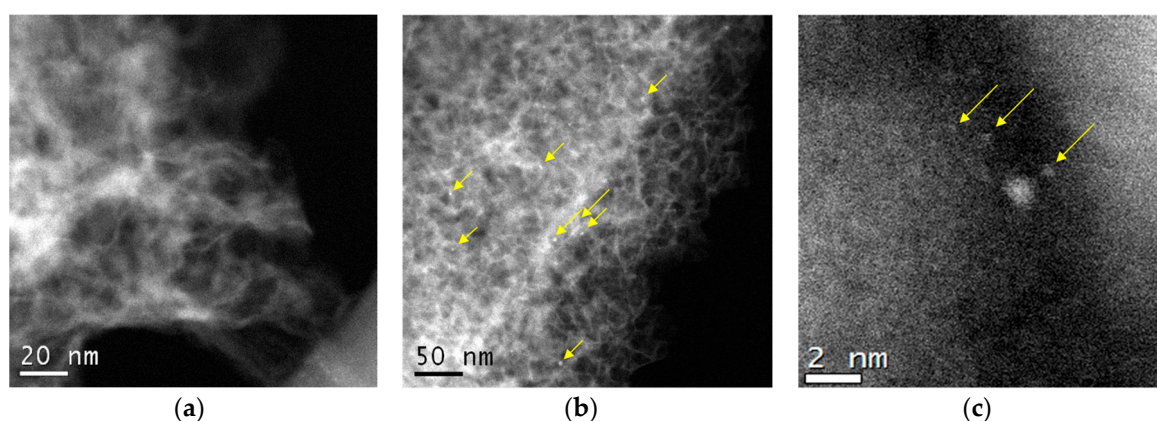


Figure 4. HAADF/STEM images of the Ni/CN-1073 catalyst after the reaction: (a) region without nanoparticles, (b) and (c) regions with nanoparticles and clusters.

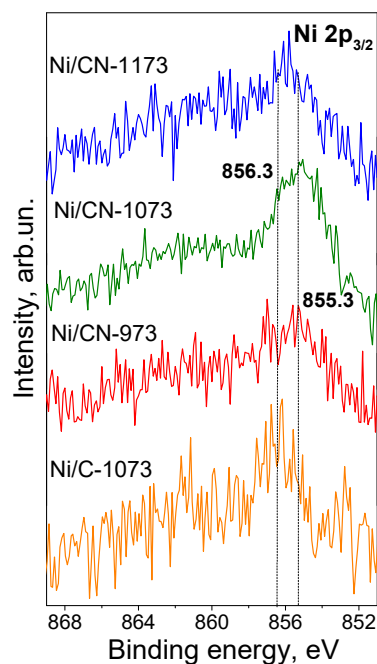


Figure 5. Ni $2p_{3/2}$ X-ray photoelectron spectra of the Ni catalysts after the reaction.

3.3. Catalytic Studies

The conversion-temperature dependences are shown in Figure 6a. At low temperatures, the Ni/CN-973, Ni/CN-1073, and Ni/CN-1173 catalysts show a higher conversion than the Ni/C-1073 catalyst. Hence, the nitrogen insertion into the support promotes the reaction. The specific reaction rates calculated at 553 K are given in Figure 6b. This graph additionally shows the effect of the synthesis temperature on the catalytic activity. Thus, the temperature of 1073 K was optimal for the catalyst synthesis from acetonitrile. Since the activity and content of pyridinic nitrogen did not differ much, the growth of the activity with nitrogen should be assigned to the appearance of nickel sites stabilized by pyridinic nitrogen sites. The obtained activity was difficult to compare with the activity reported in the literature for some supported Ni catalysts [10], since the content of Ni in our samples was by a factor of 2–22 lower and the reaction temperature was higher (533–593 K vs. 400–500 K).

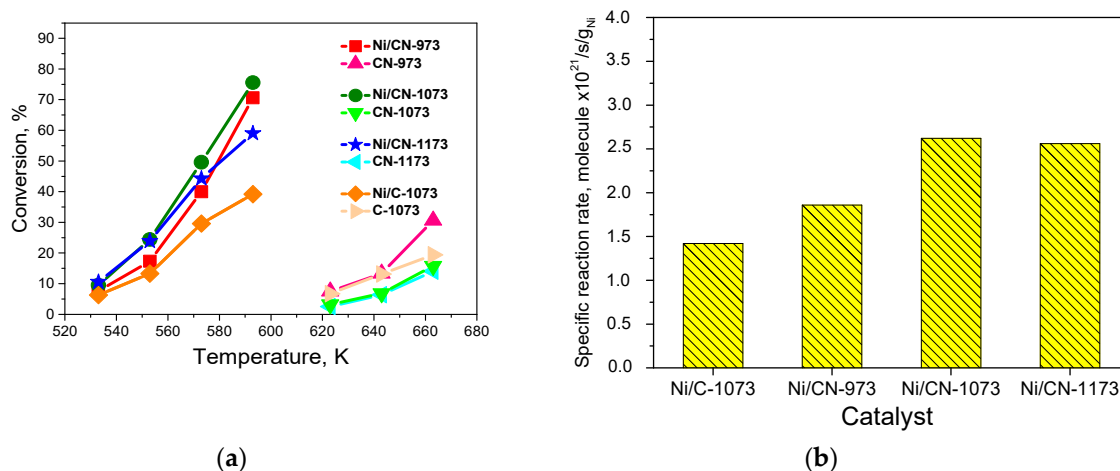


Figure 6. (a) Dependences of the formic acid decomposition conversions on temperature for the Ni catalysts (7 mg) and carbon supports (4 mg) and (b) dependence of the specific reaction rates for the Ni catalysts at 553 K.

The supports also could work as catalysts in the formic acid decomposition reaction, but not as efficiently, as Ni catalysts did (Figure 6a). At 663 K, the highest conversion was demonstrated by the CN-973 support (30%) and the lowest—by the CN-1173 support (14%). Such a spread in the conversions may be due to the differences in the specific surface areas of the supports (Table 1) and the presence of different nitrogen sites (Figure 1).

It is interesting that the activities of the Ni/CN-1073 and Ni/CN-1173 catalysts were close despite the mean Ni particle sizes were different (Table 1). It should be emphasized that used supports differed in the content of oxygen (Table 1) and in the ratio of graphitic and pyrrolic nitrogen species (Figure 1b). However, for better explanation of this result a determination of the ratio of atomic Ni species and Ni atoms present in nanoparticles is needed. DFT calculations of the formic acid interaction with different Ni structures would help also.

The apparent activation energies for the reaction over the studied catalysts were estimated from the Arrhenius plots. The obtained values were in the range of $100 \pm 9 \text{ kJ mol}^{-1}$. Interesting that the close values were obtained earlier for formic acid decomposition over unsupported Ni powder and Ni catalysts supported on silica and alumina [10] as well as for decomposition of Ni formate [27]. The determined apparent activation energies for formic acid decomposition over carbon supports without Ni were significantly higher ($125\text{--}148 \text{ kJ mol}^{-1}$).

To test the stability, the most promising catalyst Ni/CN-1073 was used. The results of the test for 5 h at 573 K are shown in Figure 7. It is seen that the hydrogen production selectivity was about 97%. The conversion demonstrates a slight increase from 57% to 61% in the time range from 20 to 60 min, but it did not change during the next 4 h. Thus, it was possible to conclude that this catalyst was quite stable and selective in the reaction, which means that there was no need to perform recycling experiments.

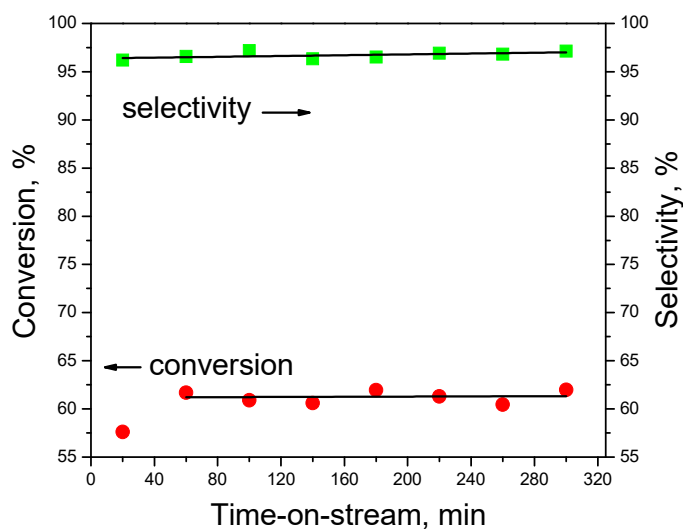


Figure 7. Stability test with the Ni/CN-1073 catalyst at 573 K.

4. Conclusions

Nitrogen-doping of the carbon support led to a significant increase of the rate of the hydrogen production from formic acid decomposition (by up to a factor of 2). The nitrogen-doped Ni catalysts showed very stable activity and high selectivity of the hydrogen production (97%). For the Ni catalysts on the nitrogen-doped supports synthesized at 973 K and 1073 K, it was difficult to find Ni containing nanoparticles by HAADF/STEM and TEM since the Ni dispersion was very high. Nickel in these catalysts was probably presented in the form of single Ni cations or few atoms clusters attached to pyridinic nitrogen of the support as was confirmed by XPS study. At the same time, the nanoparticles with a mean size of 3.9 nm were clearly observed in the Ni/C-1073 catalyst. The used nitrogen-doped

supports had no significant difference in nitrogen content. The difference was in the content of each nitrogen form. This ratio of nitrogen forms and surface area of the support determine the Ni particle size. These parameters are interconnected and for better understanding of the role of particular parameter, it is necessary to perform EXAFS studies of the Ni state in the catalysts and DFT calculations of the possible Ni structures on nitrogen-doped carbon and interaction of such structures with the formic acid molecule.

Author Contributions: Synthesis, measurements and writing, A.D.N.; characterization, O.A.S., A.V.I. and I.P.A.; funding acquisition, supervision and data curation, L.G.B. and A.V.O.; methodology, data analysis and writing, D.A.B.

Funding: This research was funded by the Russian Science Foundation, grant number 16-13-00016.

Acknowledgments: The XPS studies were conducted using the equipment of the Center of Collective Use «National Center of Catalyst Research».

Conflicts of Interest: The authors declare no conflict of interest.

Nomenclature

BET	Brunauer–Emmett–Teller
DFT	Density Functional Theory
EXAFS	Extended X-ray Absorption Fine Structure
HAADF/STEM	high angle annular dark field/scanning transmission electron microscopy
HRTEM	high resolution transmission electron microscopy
XPS	X-ray photoelectron spectroscopy

References

- Bulushev, D.A.; Ross, J.R.H. Towards Sustainable Production of Formic Acid. *ChemSusChem* **2018**, *11*, 821–836. [[CrossRef](#)] [[PubMed](#)]
- Bulushev, D.A.; Ross, J.R.H. Heterogeneous Catalysts for Hydrogenation of CO₂ and Bicarbonates to Formic Acid and Formates. *Catal. Rev.* **2018**, *60*, 566–593. [[CrossRef](#)]
- Koroteev, V.O.; Bulushev, D.A.; Chuvilin, A.L.; Okotrub, A.V.; Bulusheva, L.G. Nanometer-Sized MoS₂ Clusters on Graphene Flakes for Catalytic Formic Acid Decomposition. *ACS Catal.* **2014**, *4*, 3950–3956. [[CrossRef](#)]
- Kurnia, I.; Yoshida, A.; Situmorang, Y.A.; Kasai, Y.; Abudula, A.; Guan, G. Utilization of Dealkaline Lignin as a Source of Sodium-Promoted MoS₂/Mo₂C Hybrid Catalysts for Hydrogen Production from Formic Acid. *ACS Sustain. Chem. Eng.* **2019**, *7*, 8670–8677. [[CrossRef](#)]
- Koós, Á.; Solymosi, F. Production of CO-Free H₂ by Formic Acid Decomposition over Mo₂C/Carbon Catalysts. *Catal. Lett.* **2010**, *138*, 23–27. [[CrossRef](#)]
- Bulushev, D.A.; Chuvilin, A.L.; Sobolev, V.I.; Stolyarova, S.G.; Shubin, Y.V.; Asanov, I.P.; Ishchenko, A.V.; Magnani, G.; Riccò, M.; Okotrub, A.V.; et al. Copper on Carbon Materials: Stabilization by Nitrogen Doping. *J. Mater. Chem. A* **2017**, *5*, 10574–10583. [[CrossRef](#)]
- Pechenkin, A.; Badmaev, S.; Belyaev, V.; Sobyenin, V. Production of Hydrogen-Rich Gas by Formic Acid Decomposition over CuO-CeO₂/γ-Al₂O₃ Catalyst. *Energies* **2019**, *12*, 3577. [[CrossRef](#)]
- Bing, Q.M.; Liu, W.; Yi, W.C.; Liu, J.Y. Ni Anchored C₂N Monolayers as Low-Cost and Efficient Catalysts for Hydrogen Production from Formic Acid. *J. Power Sources* **2019**, *413*, 399–407. [[CrossRef](#)]
- Fujitsuka, H.; Nakagawa, K.; Hanprerakriengkrai, S.; Nakagawa, H.; Tago, T. Hydrogen Production from Formic Acid Using Pd/C, Pt/C, and Ni/C Catalysts Prepared from Ion-Exchange Resins. *J. Chem. Eng. Jpn.* **2019**, *52*, 423–429. [[CrossRef](#)]
- Iglesia, E.; Boudart, M. Decomposition of Formic Acid on Copper, Nickel, and Copper-Nickel Alloys: Iii. Catalytic Decomposition on Nickel and Copper-Nickel Alloys. *J. Catal.* **1983**, *81*, 224–238. [[CrossRef](#)]
- Yang, G.; Han, H.; Li, T.; Du, C. Synthesis of Nitrogen-Doped Porous Graphitic Carbons Using Nano-CaCO₃ as Template, Graphitization Catalyst, and Activating Agent. *Carbon* **2012**, *50*, 3753–3765. [[CrossRef](#)]

12. Xia, Y.; Mokaya, R. Synthesis of Ordered Mesoporous Carbon and Nitrogen-Doped Carbon Materials with Graphitic Pore Walls Via a Simple Chemical Vapor Deposition Method. *Adv. Mater.* **2004**, *16*, 1553–1558. [[CrossRef](#)]
13. Zacharska, M.; Bulusheva, L.G.; Lisitsyn, A.S.; Beloshapkin, S.; Guo, Y.; Chuvilin, A.L.; Shlyakhova, E.V.; Podyacheva, O.Y.; Leahy, J.J.; Okotrub, A.V.; et al. Factors Influencing the Performance of Pd/C Catalysts in the Green Production of Hydrogen from Formic Acid. *ChemSusChem* **2017**, *10*, 720–730. [[CrossRef](#)] [[PubMed](#)]
14. Navlani-García, M.; Mori, K.; Salinas-Torres, D.; Kuwahara, Y.; Yamashita, H. New Approaches toward the Hydrogen Production from Formic Acid Dehydrogenation over Pd-Based Heterogeneous Catalysts. *Front. Mater.* **2019**, *6*. [[CrossRef](#)]
15. Salinas-Torres, D.; Navlani-García, M.; Mori, K.; Kuwahara, Y.; Yamashita, H. Nitrogen-Doped Carbon Materials as a Promising Platform toward the Efficient Catalysis for Hydrogen Generation. *Appl. Catal. A Gen.* **2018**, *571*, 25–41. [[CrossRef](#)]
16. Yamada, Y.; Suzuki, Y.; Yasuda, H.; Uchizawa, S.; Hirose-Takai, K.; Sato, Y.; Suenaga, K.; Sato, S. Functionalized Graphene Sheets Coordinating Metal Cations. *Carbon* **2014**, *75*, 81–94. [[CrossRef](#)]
17. Liu, W.; Chen, Y.; Qi, H.; Zhang, L.; Yan, W.; Liu, X.; Yang, X.; Miao, S.; Wang, W.; Liu, C.; et al. A Durable Nickel Single-Atom Catalyst for Hydrogenation Reactions and Cellulose Valorization under Harsh Conditions. *Angew. Chem. Int. Ed.* **2018**, *57*, 7071–7075. [[CrossRef](#)]
18. Jiang, K.; Siahrostami, S.; Akey, A.J.; Li, Y.; Lu, Z.; Lattimer, J.; Hu, Y.; Stokes, C.; Gangishetty, M.; Chen, G.; et al. Transition-Metal Single Atoms in a Graphene Shell as Active Centers for Highly Efficient Artificial Photosynthesis. *Chem* **2017**, *3*, 950–960. [[CrossRef](#)]
19. Cheng, Y.; Zhao, S.; Johannessen, B.; Veder, J.-P.; Saunders, M.; Rowles, M.R.; Cheng, M.; Liu, C.; Chisholm, M.F.; Marco, R.; et al. Atomically Dispersed Transition Metals on Carbon Nanotubes with Ultrahigh Loading for Selective Electrochemical Carbon Dioxide Reduction. *Adv. Mater.* **2018**, *30*, 1706287. [[CrossRef](#)]
20. Yang, J.; Qiu, Z.; Zhao, C.; Wei, W.; Chen, W.; Li, Z.; Qu, Y.; Dong, J.; Luo, J.; Li, Z.; et al. In Situ Thermal Atomization to Convert Supported Nickel Nanoparticles into Surface-Bound Nickel Single-Atom Catalysts. *Angew. Chem.* **2018**, *130*, 14291–14296. [[CrossRef](#)]
21. Cheng, Y.; Zhao, S.; Li, H.; He, S.; Veder, J.-P.; Johannessen, B.; Xiao, J.; Lu, S.; Pan, J.; Chisholm, M.F.; et al. Unsaturated Edge-Anchored Ni Single Atoms on Porous Microwave Exfoliated Graphene Oxide for Electrochemical CO₂. *Appl. Catal. B Environ.* **2019**, *243*, 294–303. [[CrossRef](#)]
22. Zhong, W.; Liu, Y.; Deng, M.; Zhang, Y.; Jia, C.; Prezhdo, O.V.; Yuan, J.; Jiang, J. C₂N-Supported Single Metal Ion Catalysts for HCOOH Dehydrogenation. *J. Mater. Chem. A* **2018**, *6*, 11105–11112. [[CrossRef](#)]
23. Shlyakhova, E.V.; Bulusheva, L.G.; Kanygin, M.A.; Plyusnin, P.E.; Kovalenko, K.A.; Senkovskiy, B.V.; Okotrub, A.V. Synthesis of Nitrogen-Containing Porous Carbon Using Calcium Oxide Nanoparticles. *Phys. Status Solidi B* **2014**, *251*, 2607–2612. [[CrossRef](#)]
24. Golub, F.S.; Beloshapkin, S.; Gusel'nikov, A.V.; Bolotov, V.A.; Parmon, V.N.; Bulushev, D.A. Boosting Hydrogen Production from Formic Acid over Pd Catalysts by Deposition of N-Containing Precursors on the Carbon Support. *Energies* **2019**, *12*, 3885. [[CrossRef](#)]
25. Okotrub, A.V.; Fedorovskaya, E.O.; Senkovskiy, B.V.; Bulusheva, L.G. Nitrogen Species in Few-Layer Graphene Produced by Thermal Exfoliation of Fluorinated Graphite Intercalation Compounds. *Phys. Status Solidi B* **2015**, *252*, 2444–2450. [[CrossRef](#)]
26. Berríos, C.; Cárdenas-Jirón, G.I.; Marco, J.F.; Gutiérrez, C.; Ureta-Zañartu, M.S. Theoretical and Spectroscopic Study of Nickel(II) Porphyrin Derivatives. *J. Phys. Chem. A* **2007**, *111*, 2706–2714. [[CrossRef](#)]
27. Iglesia, E.; Boudart, M. Decomposition of Formic-Acid on Copper, Nickel, and Copper Nickel-Alloys. IV. Temperature-Programmed Decomposition of Bulk Nickel Formate and of Formic-Acid Preadsorbed on Nickel Powder. *J. Catal.* **1984**, *88*, 325–332. [[CrossRef](#)]

